Robust Formation of Optimal Single Spheroids towards Cost-Effective In-Vitro 3-Dimensional Tumor Models

Kinana Habra
Nottingham Trent University
Joshua R.D. Pearson
Nottingham Trent University
Stéphanie E. B. McArdle (stephanie.mcardle@ntu.ac.uk)
Nottingham Trent University

Article

Keywords: carnosine, glioblastoma, prostate cancer, breast cancer, 3-D model, single spheroid, high throughput, U87 MG.

Posted Date: June 1st, 2022

DOI: https://doi.org/10.21203/rs.3.rs-1695738/v1

Robust Formation of Optimal Single Spheroids towards Cost-Effective *In-Vitro* 3-Dimensional Tumor Models

Kinana Habra [1,2], Joshua R.D. Pearson[2,3], Stéphanie E. B. McArdle [2,3*]

[1] Chemistry department, School of Science and Technology, Nottingham Trent University, Nottingham NG11 8NS, UK.

[2] John van Geest Cancer Research Centre, School of Science and Technology, Nottingham Trent University, Nottingham NG11 8NS, UK.

[3] Centre for Health, Ageing and Understanding Disease, School of Science and Technology, Nottingham Trent University, Nottingham, UK

[*]Correspondence: stephanie.mcardle@ntu.ac.uk; Tel.: +44 115 84 83136

Abstract

Monolayer cell cultures, while useful for basic *in vitro* studies, are not physiologically relevant. Spheroids, a complex 3-dimensional (3D) structure resemble *in vivo* tumor growth more closely thereby allowing results obtained with spheroids relating to proliferation, cell death, differentiation, metabolism, and various anti-tumor therapies to be more predictive of *in vivo* outcomes. The protocol herein presents a rapid and high throughput method for the generation of single spheroids using various cancer cell lines including (U87 MG, SEBTA-027, SF188) brain cancer cells, (DU-145, TRAMP-C1) prostate cancer cells, and (BT-549, Py230) breast cancer cells in a 96-round bottom well plates. The proposed method is associated with significantly low costs (*ca.* £1) per plate without the need for refining or transferring and homogeneous compact spheroid morphology was evidenced as early as 1 day after following this protocol. By using confocal microscopy and the IncuCyte live imaging system, proliferating cells were traced in the rim while dead cells were found to be located inside the core region of the spheroid. H&E staining of spheroid sections was utilized to investigate the tightness of the cell packaging and Western blotting analyses revealed that these spheroids adopted a stem cell-like phenotype. This method was also used to obtain EC50 of the anti-cancer dipeptide carnosine on U87 MG 3D culture. The affordable easy-to-follow 5 step-protocol allows for robust generation of various uniform spheroids which show 3D morphology characteristics.

Keywords: carnosine; glioblastoma; prostate cancer; breast cancer; 3-D model; single spheroid; high throughput; U87 MG.

Introduction

Three-dimensional models have been shown to have many advantages over monolayer cell systems. Spheroids have attracted attention due to their complex microenvironment and behavior which mimic many of the natural *in vivo* conditions[1]. While single spheroids cannot replace *in vivo* models' scientific investigation, they represent a valuable bridge between monolayer cell studies and the more complicated structure of *in vivo* tumors[2]. Spheroid formation has shown potential for high-throughput investigations of anti-cancer treatments[3]. The current standard methods for spheroid generation include the liquid-overlay[4], hanging-drop[5], and shaking methods[6,7]. The limitations of these methods were found in the amount of spheroid formation and the relative excessive costs. Some commercially available examples are Corning®, Costar®, and Brand® ultra-low attachment 96 or 24 well plates and the Kuraray® multiple pore type which all have the same basic principle. Other methods such as magnetic levitation[8], NASA Bioreactor[9], and micro-cages require expensive tools while the uniformity of the generated spheroids remains low[10]. Therefore, a method that would combine the reproducibility of forming copious quantities of uniform spheroids while keeping the costs low is required. Herein, we describe a detailed cost-effective protocol for establishing an *in vitro* 3D single spheroid model which can be used to identify potential new therapeutic approaches. We have shown that the method can be applied to many human and murine cancer cell lines of different origins (prostate cancer, TNBC, and GBM). More specifically we have shown that the formation of spheroids, i.e., when the cells stop shrinking and started to grow is cell-type dependent and will need to be optimized for each cell line these can then be utilized for the investigation of targeted drugs, antibodies, and immunoconjugates[11]. In addition, using U87 MG cells, a conventional glioblastoma cell line most studied due to its tumor stem cell-like features[12–14], as an example, we have generated single spheroids and assessed the effect of carnosine, an anti-tumor di-peptide, which has the potential to be used as a sustained-release therapy of glioblastoma[6,11,15,16].

Materials and methods

Cell Culture

The human glioblastoma U87 MG-Red-FLuc cells (Bioware Brite, PerkinElmer, Waltham, Massachusetts, USA) were incubated in Opti-MEM Reduced Serum Medium (Gibco™, Thermo

62 Fisher Scientific, Waltham, Massachusetts, USA) culture medium, supplemented with fetal
63 bovine serum up to 10%. The antibiotic puromycin (Gibco®, Thermo Fisher Scientific Waltham,
64 Massachusetts, USA) was added after the initial thaw at 2 µg/mL. The incubation was at 37˚C
65 in a humidified atmosphere containing 5% CO_2. Other cell lines were cultured in their specific
66 media by following the same protocol outlines. The human Glioblastoma SEBTA-027
67 (Recurrent GBM cell line derived from the right parieto-occipital region of a 59-year-old
68 female) and SF188 (GBM cell line derived from an 8-year-old male) were cultured in Gibco™
69 DMEM, high glucose, GlutaMAX™ Supplement, and 10% fetal calf serum (Gibco™, Thermo
70 Fisher Scientific, Waltham, Massachusetts, USA). Both cell lines were a generous gift from the
71 University of Portsmouth, neuro-oncology group. The human Prostate cancer DU145, HTB-
72 81™ (American Type Culture Collection ATCC, Virginia, USA) were cultured in Eagle's minimum
73 essential medium modified to contain Earle's Balanced Salt Solution, non-essential amino
74 acids, 2 mM L-glutamine, 1 mM sodium pyruvate (BioWhittaker® Medium EMEM Cell Culture
75 Media, Lonza, Maryland, USA), and 10% fetal calf serum. The murine prostate cancer TRAMP-
76 C1 (C57Bl/6 mice cells which are derived from prostate adenocarcinoma cells from TRAMP
77 mice) were cultured in Dulbecco's Modified Eagle Medium 4.5 g/L glucose w/L-Gln w/ sodium
78 pyruvate (DMEM, Lonza, Maryland, USA), and 10% fetal calf serum. This cell line was provided
79 by Matteo Bellone (University of Milan, Milan, Italy). The human breast cancer BT-549 is
80 ductal carcinoma (American Type Culture Collection ATCC, Virginia, USA) was cultured in
81 Corning RPMI 1640 Medium with L-Glutamine (Corning™ RPMI 1640 Medium, New York, USA),
82 10% fetal calf serum and 0.023U/mL insulin. The murine breast adenocarcinoma Py230
83 (American Type Culture Collection ATCC, Virginia, USA) was cultured in Corning Medium F-
84 12K with L-glutamine (BioWhittaker® Medium F12K Medium, Lonza, Maryland, USA), and 10%
85 fetal calf serum, 0.1% MITO+ serum extender (Corning®, New York, USA).

86 **The protocol of spheroids generation**

87 1- A volume of 50 µl of anti-adherence rinsing solution (STEMCELL Technologies, Cambridge,
88 UK) was added to each well of a 96-well round-bottom hydrophobic tissue culture plate
89 with a growth surface for suspension (Green code: 83.3925.500, Sarstedt, Nümbrecht,
90 Germany).[17]
91 2- After 15 minutes, the solution was discarded then each well was washed with 50 µl of
92 serum-free media.

3- The cells were grown as a monolayer and when the cells reached 70–80% confluence, they were sub-cultured using 0.05% Trypsin−0.53 mM EDTA (Sigma-Aldrich, St. Louis, Missouri, USA) for cell detachment.
4- To generate a single-cell suspension, the cells were seeded (400 cells/well/100 µl full media).
5- Directly, the spheroid formation was initiated by centrifuging the plates with a benchtop centrifuge (Eppendorf 5810R Centrifuge, Hamburg, Germany) at 2454 rcf (3700 rpm) for 10 minutes.

The plates were incubated between 1 and 12 days under standard cell culture conditions at 37° C, and 5% CO_2 in humidified incubators. The full media had been replaced each other day and post-seeding cellular phenotype was checked by the microscopical observable physical properties of each spheroid including the appearance, development, and behavior.

Localization of dead and proliferating cells within spheroids

The seeded cells were stained by IncuCyte® Cytotox red for counting dead cells (250 nM, Essen Bioscience) and the generated spheroids were transferred to the IncuCyte S3 Live-Cell Analysis System (Essen Bioscience Inc., Ann Arbor, Michigan, USA). Live images were snapped with 4× objective lenses in each well every hour inside an incubator over 12 days. The culture medium was replaced every 2 days for maintaining the spheroid's survival. The localization of the red dead cells within the spheroids was assessed by phase-contrast images using the red channel to evaluate the real-time cell membrane integrity and cell death. The total phase and the red fluorescent areas with mask were quantified for different days using IncuCyte® spheroid analysis software (Version. 2020B, Essen Bioscience Inc., Ann Arbor, Michigan, USA).

Imaging studies

The single spheroids were stained following the instructions of each kit. The dead cells were stained by IncuCyte® Cytotox red for counting dead cells (250 nM, Essen Bioscience) during the generation process. The cyanine nucleic acid dye permeated cells with compromised cell membranes. The green dye CFSE Cell Division Tracker Kit (BioLegend, San Diego, California, USA) and DAPI (Sigma-Aldrich, St. Louis, Missouri, USA) were used to stain the live cells and the nucleus before taking pictures. The morphology of the spheroids was assessed and recorded using the IncuCyte S3 Live-Cell Analysis System and confocal laser scanning

123 microscope (Leica, Wetzlar, Germany) by a 5× objective using the following settings:
124 sequential scanning, ex/em: Mitotracker: 543/599 nm, Hoechst: 405/461 nm. The size of the
125 spheroids was analyzed using IncuCyte® spheroid analysis software (Version. 2020B, Essen
126 Bioscience Inc., Ann Arbor, Michigan, USA), and ImageJ Software (Version. 1.44, National
127 Institute of Mental Health, Bethesda, Maryland, USA).

128 **Hematoxylin and eosin H&E stain of spheroid cross sections**

129 U87 MG spheroids were generated from 400 cells. Prior to staining, spheroids were cultivated
130 individually after 1, 3, 5, 7, and 10 days washed once in phosphate-buffered saline (Corning®,
131 Phosphate Buffer Solution (PBS), New York, USA) then fixed with 10% formalin (Merck,
132 Darmstadt, Germany). The spheroids were washed in PBS and transferred to disposable
133 biopsy embedding molds to encapsulate them with Epredia™ HistoGel™ Specimen Processing
134 Gel (Fisher-Scientific, UK). Each gel-coated spheroid was moved to a cassette and loaded
135 inside a tissue processor (Excelsior AS, Thermo Scientific, Germany). The program was set to
136 start with 6 times 70% ethanol, then 3 times xylene, and 3 times histology wax. Each cycle
137 time was 10 minutes. Then the capsules were embedded in paraffin using (Histostar, Thermo
138 Scientific, Germany) with a temperature range of -3 ˚C to -12 ˚C. Microtone (Leica, RM2235)
139 sections of 5 µm were placed on Super Frost glass slides (Menzel-Glaser, Thermo Science,
140 Germany) and allowed to dry for 2 hours at 37° C. The sections were deparaffinized by 2
141 changes of xylene for 5 min, rehydrated by 2 changes of 100% ethanol, followed by washing
142 in 70% ethanol for 1 min. After a short single rinse in distilled water, the sections were stained
143 for 20 min in Mayer's hematoxylin (Merck) and placed for 20 min under running tap water,
144 then dipped in 1% Scott's Tap. The slides were observed under the microscope. Sections were
145 counterstained with eosin (Merck) for 2 min, rinse quickly in tap water, dehydrated by a dip
146 in 70% ethanol, followed by 2 changes in 100% ethanol for 2 min each, and 2 changes of
147 xylene for 2 min. The slides were mounted in DPX (Sigma-Aldrich, Germany), and left to air
148 dry for 2 hours. spheroid sections were assessed by bright field microscopy.

149 **Immunoblotting**

150 A confluent flask (70–80%) of U87 MG cells grown in monolayer culture served as a control.
151 After 10 days, spheroids were pooled from the plate. All spheroids were washed twice with
152 ice-cold PBS (Phosphate Buffer Solution), then lysed in 500 µl RIPA lysis buffer (50 mM Tris-

153 HCl pH 8, 150 nM sodium chloride, 0.1% sodium dodecyl sulfate (SDS), 0.5% sodium
154 deoxycholate, 1% Triton x100, 1 mM EDTA) containing protease inhibitor cocktail (Sigma). The
155 lysates were vigorously vortexed and placed on the ice every 10 minutes for a 30-minute
156 period. After using the vortex mixer, the samples were centrifuged for 15 min at 15,000 rpm
157 at a temperature of 4°C. The protein concentration was determined by a BCA protein assay
158 (Sigma). A total of 20 µg protein extract was mixed with 5× Laemmli loading buffer (50%
159 glycerol, 10% SDS, 0.25% bromophenol blue, 250 mM Tris-HCl pH 6.8, 5% β-mercaptoethanol)
160 resolved on a 10% SDS-PAGE gel and a wet transfer was performed with 25 mM Tris, 192 mM
161 glycine and 20% methanol for 90 minutes at 100 V onto a nitrocellulose membrane.
162 Membranes were then blocked with a 5% milk in TBST solution and then probed with primary
163 antibodies directed against β-actin (Sigma) and vimentin (Cell Signaling Technologies). After
164 incubation with primary antibodies, HRP-linked secondary antibodies (Cell Signaling
165 Technologies) were used to detect bound primary antibodies in combination with Clarity
166 Western ECL substrate (BioRad Laboratories). The intensity of the Western blot bands was
167 quantified using ImageJ software and the expression of vimentin was expressed as the
168 intensity of the vimentin band/the intensity of the beta-actin loading control band.

169 **Statistical Analysis**

170 Three independent experimental replicates were made on each data set and the data were
171 presented as the mean ± the standard error of the mean. The one-way analysis of variance
172 (ANOVA) was carried out for multiple comparisons between the control and each group using
173 Dunnett's post-test. The value 0.05 was selected as the statistical significance level and
174 indicated with (*) for $p < 0.05$, (**) for $p < 0.01$, (***) for $p < 0.001$ and (****) for $p < 0.0001$.

175 **Results**

176 The protocol was applied to evaluate the homogeneity of growing single-well spheroids, and
177 the size distribution was quantified by the IncuCyte spheroids software[18]. The cells were
178 seeded in 3 wells (Triplicate 1-3) of a 96-well plate, and an additional well was used as control
179 (i.e., no washing referred to as triplicate 4) these were left to grow for seven days to form
180 spheroids while being monitored hourly. The mean confluence of the phase area for
181 individual spheroids was calculated using the IncuCyte spheroid software. This setting was
182 then repeated 2 more times keeping the same position for all triplicates.

183 The results demonstrated that following the protocol single spheroid could be obtained with
184 consistent reproducibility for triplicates 1, 2, and 3, while triplicate 4 failed to convert the cells
185 into spheroids instead aggregates were formed, highlighting the importance of the washing
186 step. The cells in triplicates 1-3 gathered over the first day as detected by a reduction in the
187 number of largest brightfield area (Fig 1). Thereafter, unlike the aggregates seen in triplicate
188 4, the spheroids displayed a regular morphology with a uniform spherical geometry and a
189 narrow size deviation. For U87MG cells seeding 400 cells per well on day 0 was sufficient to
190 convert them into homogeneous spheroids that ranged in diameter from 216 ± 9 µm after 1
191 day to 475 ± 8 µm after 5 days and then 847 ± 11 µm after 7 days. The homogeneity of the
192 spheroids was reflected by the small standard deviation ranging from the mean (Fig 1).

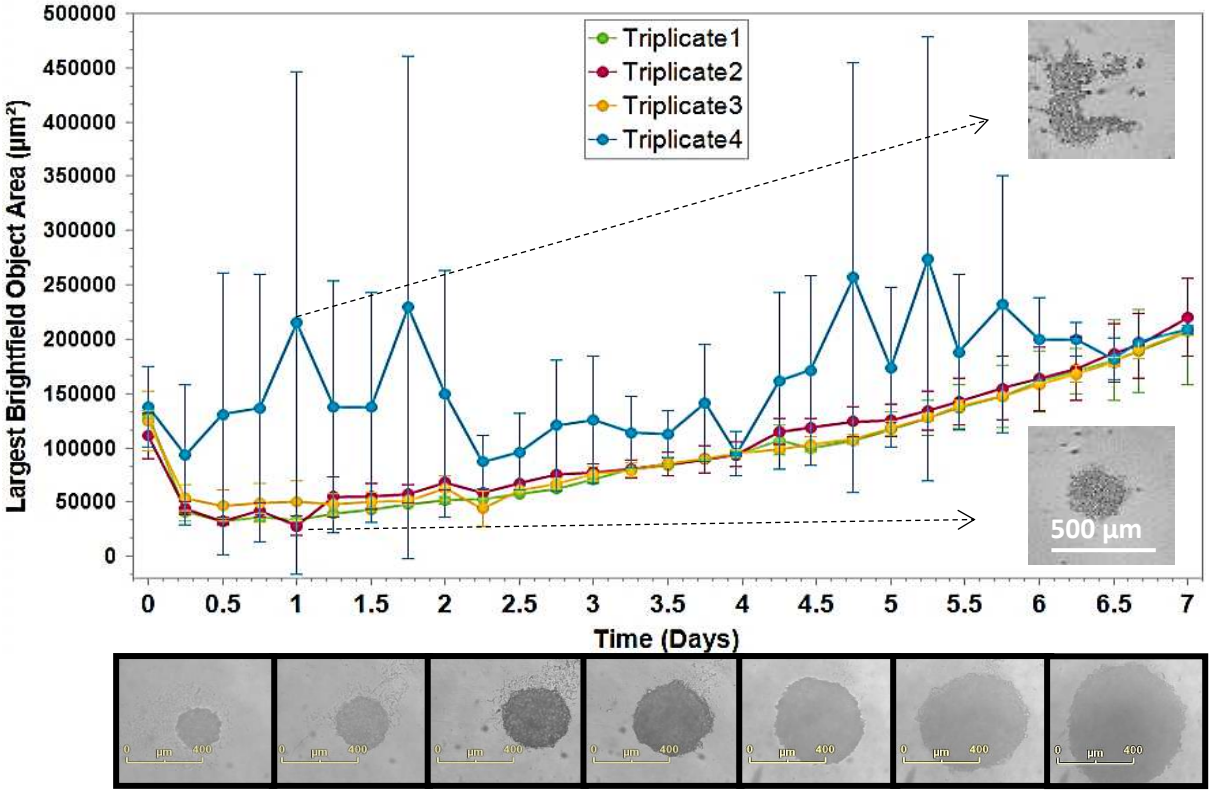

193

194 **Figure 1. IncuCyte S3 live-cell system (4×) Live spheroids images analysis shows** the proliferation curves of the
195 confluence ratio of U87 single spheroid upon using the protocol steps. The first triplicate failed to convert the
196 aggregates to spheroids without using the washing solution. However, following the protocol showed consistent
197 reproducibility for the single spheroids on three triplicates 2, 3, and 4. The images show the difference on day 1
198 between the shape of the aggregates and the successful shape of the spheroid (scale bar = 500 nm). Also, the
199 series of images below the graph shows the growth of the spheroids from day 1 to day 7 (scale bar = 400 nm).

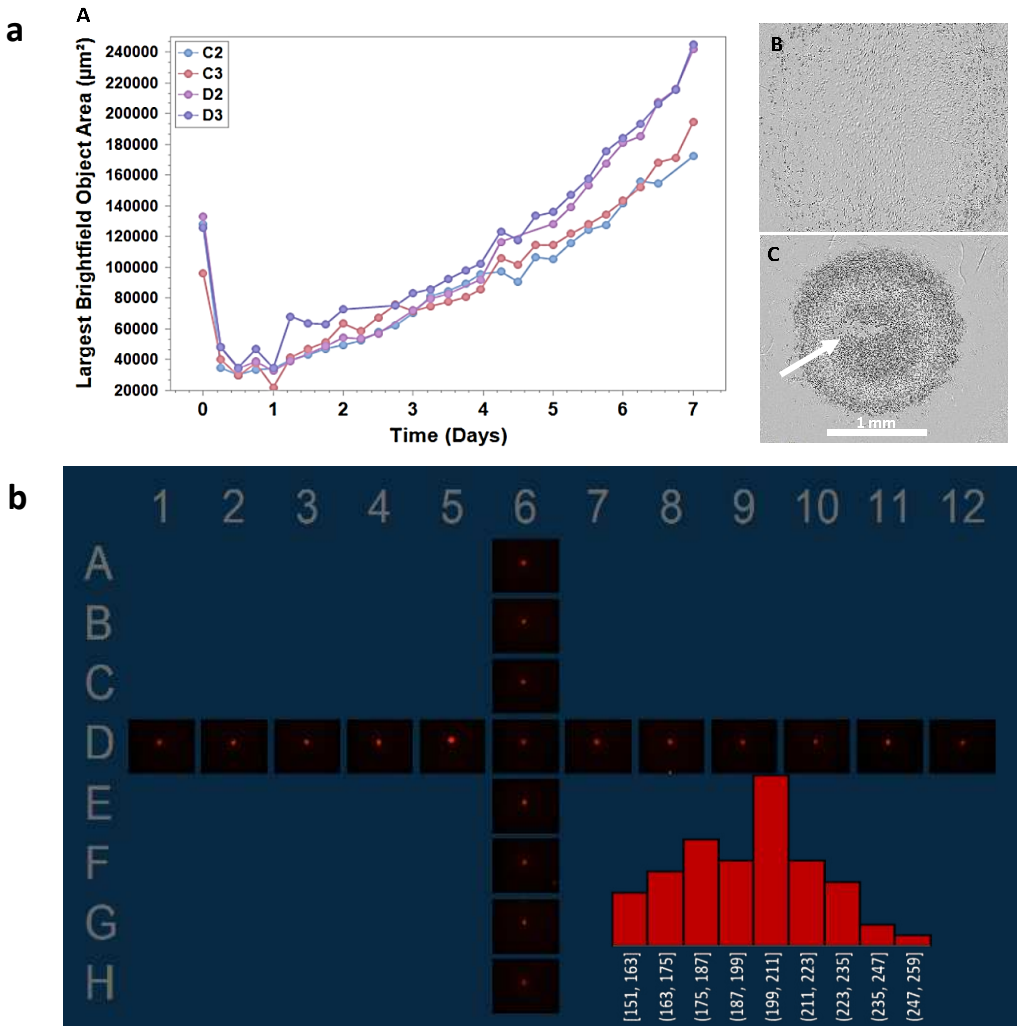

Figure 2. IncuCyte S3 live-cell system (4×) Live spheroids images analysis shows (a) A. the proliferation curves of individual U87 single spheroid from individual locations in the 96 well plate (C2, C3, D2, D3). The spheroids area decreased during the first day then each tight spheroid grew over 7 days. **B.** The instant adherence of the cells when skipping the step without washing. **C.** The cells were gathered when the anti-adherence solution was used with a 96-well round-bottom standard growth surface for adherent cells (red code), however, a crack appeared in the gathered cells after the centrifugation. In B & C cases the cells stayed as aggregates. **(b)** 96 well plate image shows the U87 cells turned into spheroids in various locations horizontally and vertically after 1 day with a size distribution is 216 ± 9 nm for individual triplicates.

In addition to washing another critical factor to consider was the type of plate used. Indeed, the use of a 96-well round bottom plate with a hydrophobic surface designed for suspension cells (Green code: 83.3925.500, Sarstedt, Nümbrecht, Germany) proved to be a key step, which promoted the formation of homogenous spheroids. By contrast, single spheroids could not be generated using a 96-well round bottom with a standard growth surface for adherent cells (Red code: 83.3925, Sarstedt, Nümbrecht, Germany) despite washing the surface of the

wells with the anti-adherence solution. The cells adhered to the bottom of the wells forming an incomplete circle after centrifugation (Fig 2, a/B & C). The most critical steps in the protocol were the use of the green code plate and the anti-adherence washing solution which consists of an amphipathic component to prevent cell adhesion[19]. This method showed cells forming spheroids in every seeded well at various locations horizontally and vertically. This monitoring confirmed the consistency and reproducibility of producing spheroids in the 96 wells (Fig 2, b).

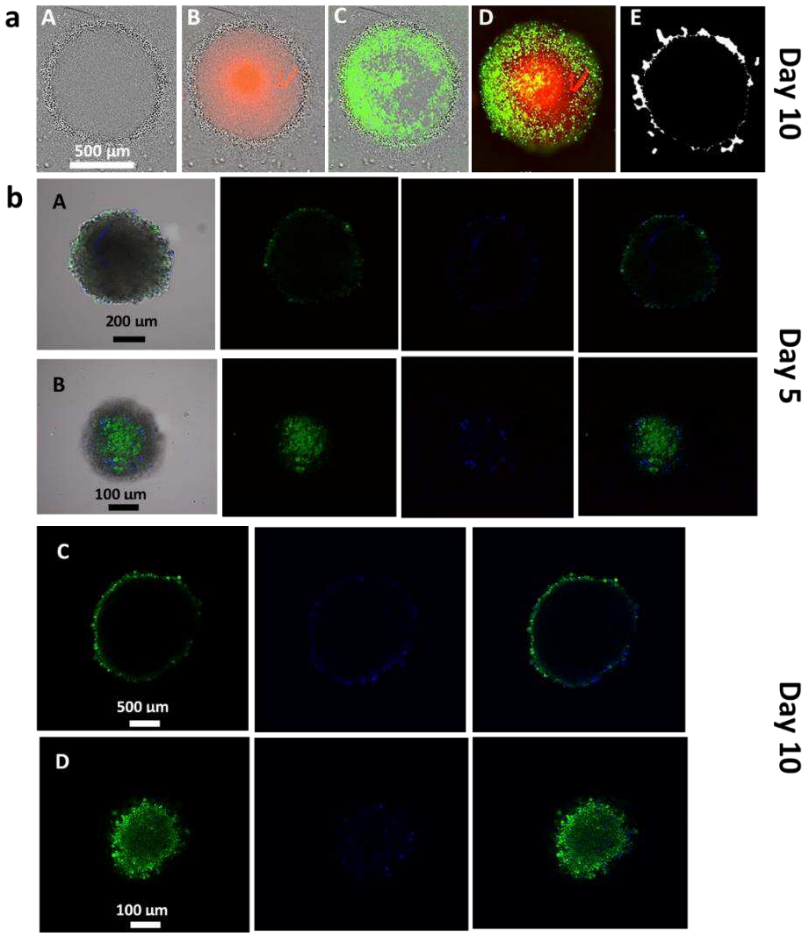

Figure 3. Fluorescence cell Imaging (a) IncuCyte S3 live-cell system (4×) Live spheroids images after 10 days. **A.** The phase image shows the confluence of the live cells around the spheroid distributed uniformly, **B.** The phase with a red channel filter image shows the localization of the dead cells in the center of the spheroid. **C.** The phase with a green channel filter image shows the 3D localization of the live cells around the spheroid. **D.** The overlap of the red and green channels shows the 3D shape of the cells dead/ live in the same spheroid. **E.** The mask of the invasion area. **(b)** Confocal images show the distribution of the green live cells and the blue nucleus which are located close to the rim of the spheroid. **A & C.** The 5- and 10- days spheroid images across the center show the dark shade of the dead cells. **B & D.** The 5- and 10-days spheroid images for the proliferating cells across the rim area.

232 The spheroids obtained were further characterized using the IncuCyte live-cell imaging
233 system. The 3D structure of the spheroids was shown to be achieved uniformly in all seeded
234 wells. The spheroids grew consistently for up to 12 days. The observed morphology confirmed
235 the overall transformation from forming aggregates to generating tight single spheroids
236 where the dead cells (stained in red) were localized in the center and the live cells proliferated
237 at the rim of the spheroid. The IncuCyte images with a green channel filter showed the live
238 CFSE stained cells surrounding the Cytotox red color which was taken up by dead cells at the
239 core of the spheroid (Fig 3, a/ A-D). This has the advantage of assessing the mobility of the
240 tumor cells and it enables the monitoring of the invasion of the U87 MG cells from the surface
241 of the spheroid. The invasion area was estimated after applying an invasion mask and
242 subtracting the area of the dead cells from the whole spheroid (Fig 3, a/ E). The confocal
243 microscopic images for the spheroid morphology showed a significant increase in growth
244 from day 5 which was confirmed by the viability of the cells at the rim of the spheroid (CFSE
245 green live cells and DAPI blue nucleus). The 5- and 10- days spheroid images across the center
246 showed the dark shade where the dead cells are located (Fig 3/ A-D).

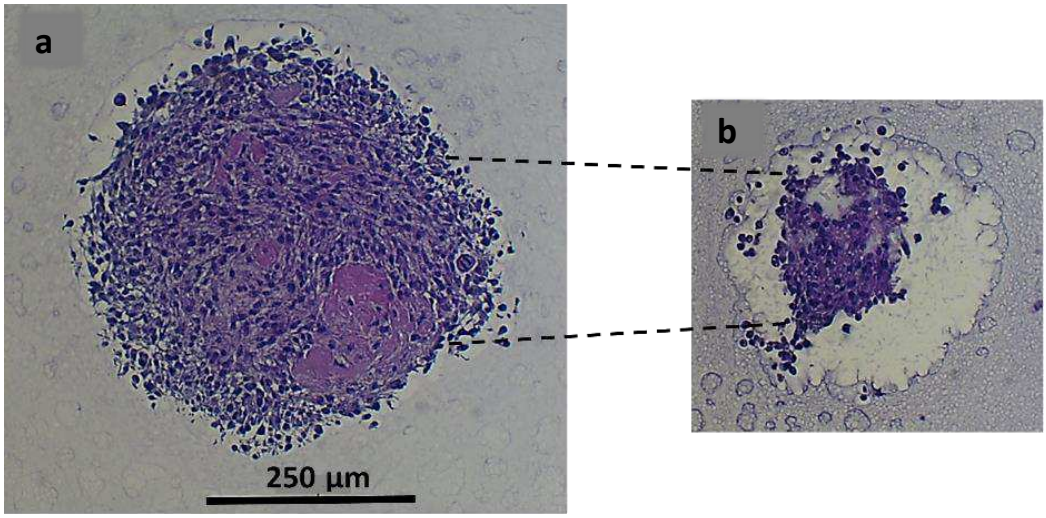

247

248 **Figure 4. Cell tightness and interaction analysis of U87 MG spheroids** H&E stain of spheroid cross-sections from
249 **(a)** the core area, and **(b)** top rim area of 7 days spheroid generated from 400 cells.

250 To investigate the tightness of the cell packaging in the single spheroid, histological sections
251 were examined for spheroids which were grown for 7 days in culture. H&E staining was
252 applied to these spheroids after fixation and embedding. The hematoxylin stains cell nuclei a
253 purplish-blue color, while eosin stains the extracellular matrix and cytoplasm pink. Figure 4
254 shows the H&E stain from the center and the rim cross-section of a spheroid. This evidenced

255 that the cell density was high in the core region, whereas the daughter cells gathered around
256 the rim to tighten and increase the spheroid size.

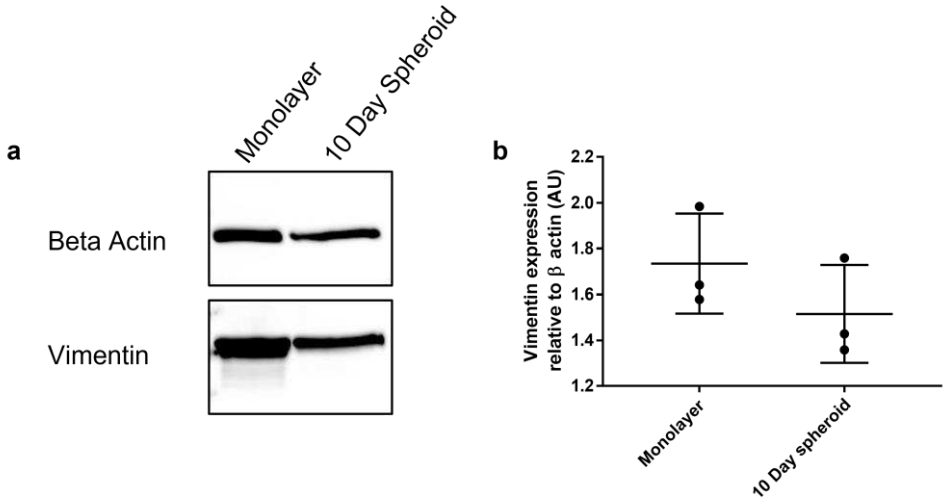

257

258 **Figure 5. Western blotting analysis of vimentin expression (a)** Representative Western blot result for vimentin
259 and Beta Actin and Vimentin obtained from U87MG cells grown either in a monolayer or as spheroids generated
260 from 400 cells for 10 days. **(b)** Quantification of vimentin expression relative to beta-actin as detected by
261 Western blotting of lysates from monolayer cultures and spheroid cultures across 3 different passages. Full
262 images of all Western blots can be seen in Figure S1.

263 The adhesion and tight junction proteins are the principal factors involved in turning cell
264 aggregates into spheroids. Western blotting revealed downregulation of vimentin in spheroid
265 cultures compared to cells grown as a monolayer (Fig 5). These findings imply that these
266 spheroids adopt a highly invasive mesenchymal phenotype as opposed to an epithelial
267 phenotype[20]. This epithelial to mesenchymal transition (EMT) has previously been identified
268 in spheroids formed using the CAL33 head and neck squamous cell carcinoma[21]. These EMT
269 changes are indicative of a cancer stem cell phenotype; a population known to be highly
270 treatment-resistant and responsible for tumor recurrence[22]. As a result of these findings, the
271 proposed technique represents an excellent *in vitro* single spheroid model for testing
272 potential therapies as a preliminary platform before moving to *in vivo* mouse models.

273 The applicability and reproducibility of this method were demonstrated using different cell
274 lines from various cancer types (originating from either humans or mice) (Fig 6).

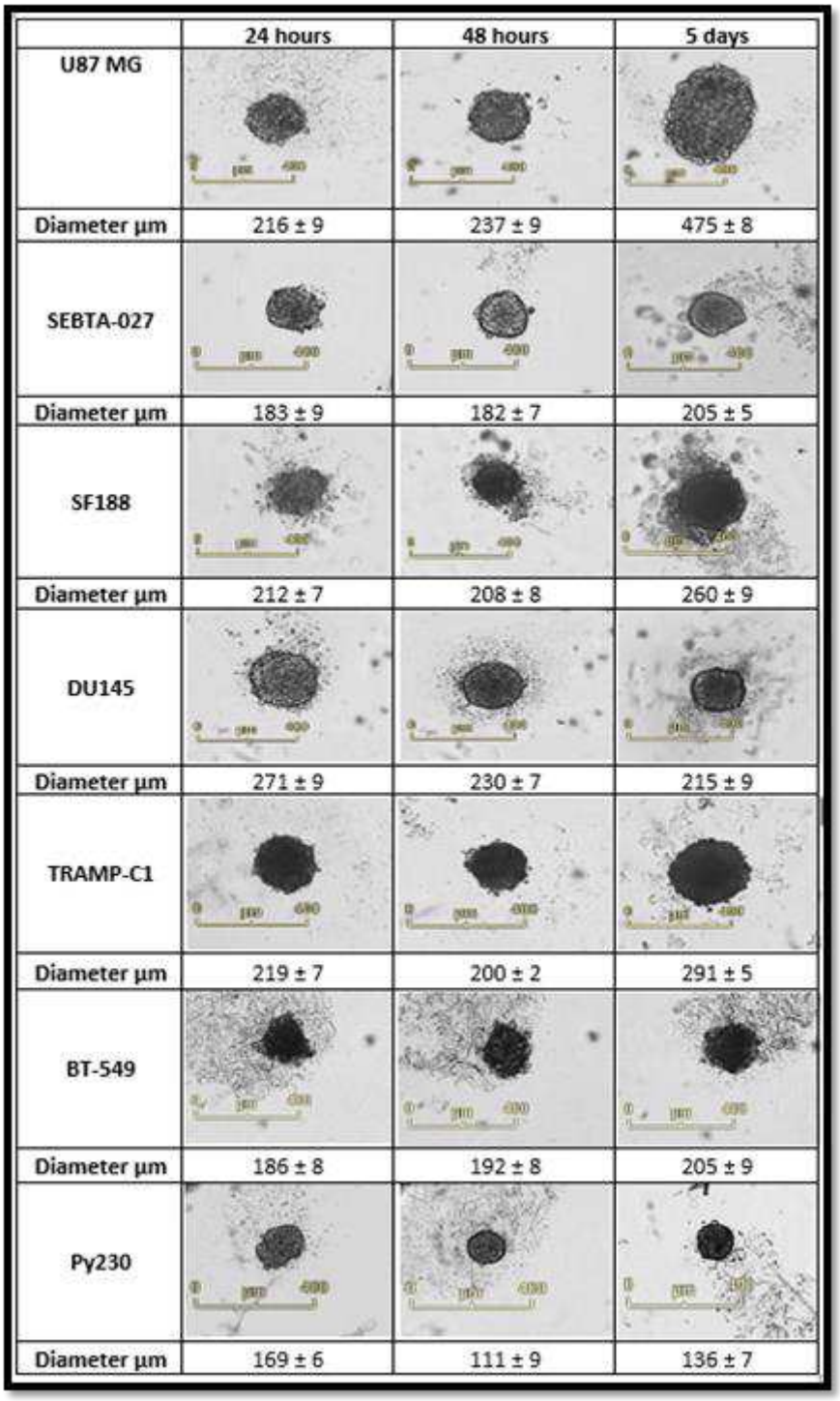

Figure 6. IncuCyte S3 live-cell system (4×) live spheroids images show the potential of using the protocol to obtain single spheroids from various cell lines.

In addition, the efficacy of an anti-tumor dipeptide known as carnosine was applied at different concentrations (0, 50, 100, 150 mM) to U87 MG grown as single spheroids, on days 1, 3, and 5 to mimic sustained-release therapy. The change in morphology of the single spheroids after day 3 proved the effect of carnosine in suppressing the proliferation of these

282 spheroids. From the series of carnosine concentrations, the critical amount to hinder the
283 spheroid growth was found to be over 100 mM (Fig 7).

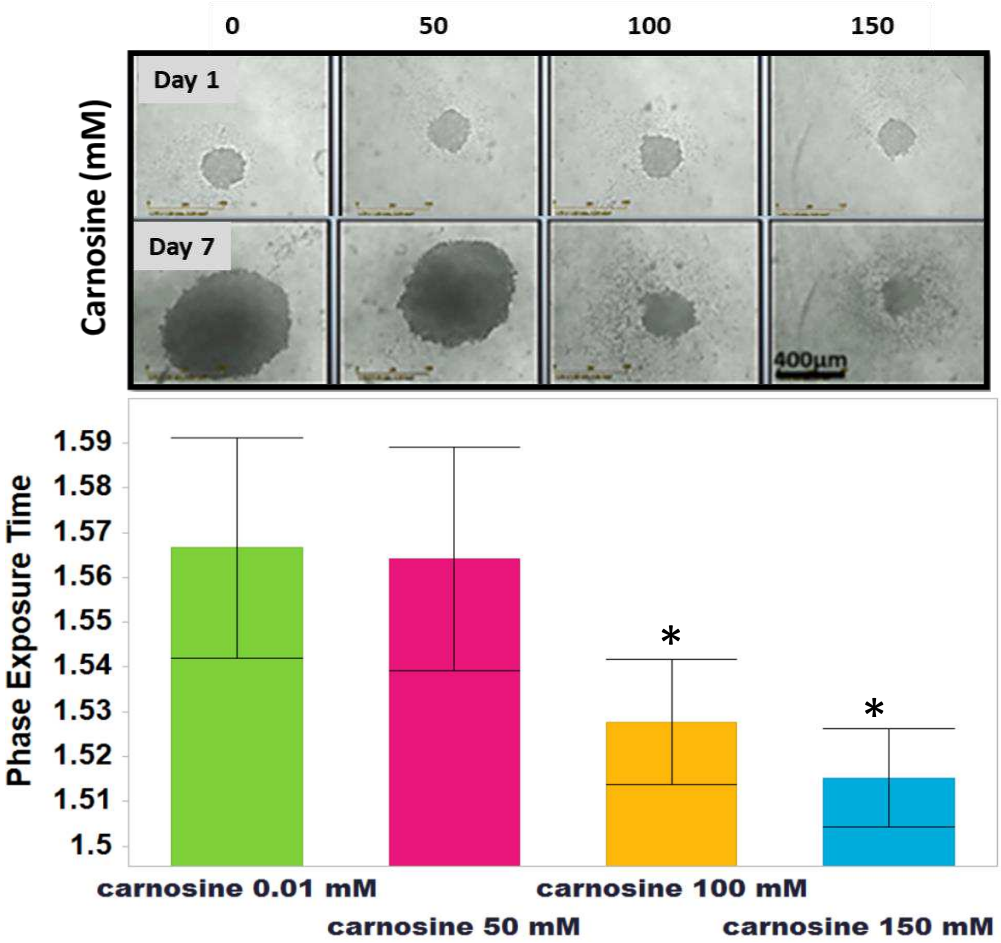

284

285 **Figure 7. IncuCyte S3 live-cell system** (4×) live spheroids images show the comparison between the morphology
286 and size of single spheroids on day 1 and day 7 after applying frequent doses of carnosine treatment. The
287 spheroid growth and tightness were affected by the mimicked sustained release of carnosine concentration ≥
288 100 mM and a significant difference was reported in phase exposure. The statistical significance level on day 7
289 indicated with (*) for $p < 0.05$, (**) for $p < 0.01$. Error bars represent the standard error of the mean (SEM).

290 Interestingly, the concentration of carnosine required to affect the viability of U87 MG was
291 found to be around 30 mM in a previous investigation that utilized a monolayer 2-D model[15].
292 The same results were obtained in Figure 8 at 22 hours when EC50 was calculated before the
293 complete tightness of the cell spheroid. Comparing drug sensitivity in 2D and 3D cultures was
294 feasible daily by measuring EC50 using the change of spheroids phase exposure. The
295 increment of EC50 on day 2 to 155 mM was an important indicator to add the second
296 carnosine dose on day 3. The EC50 was stable at around 100 mM between days 3 and 7 which
297 confirmed the suitability of the dose frequency (Fig 7).

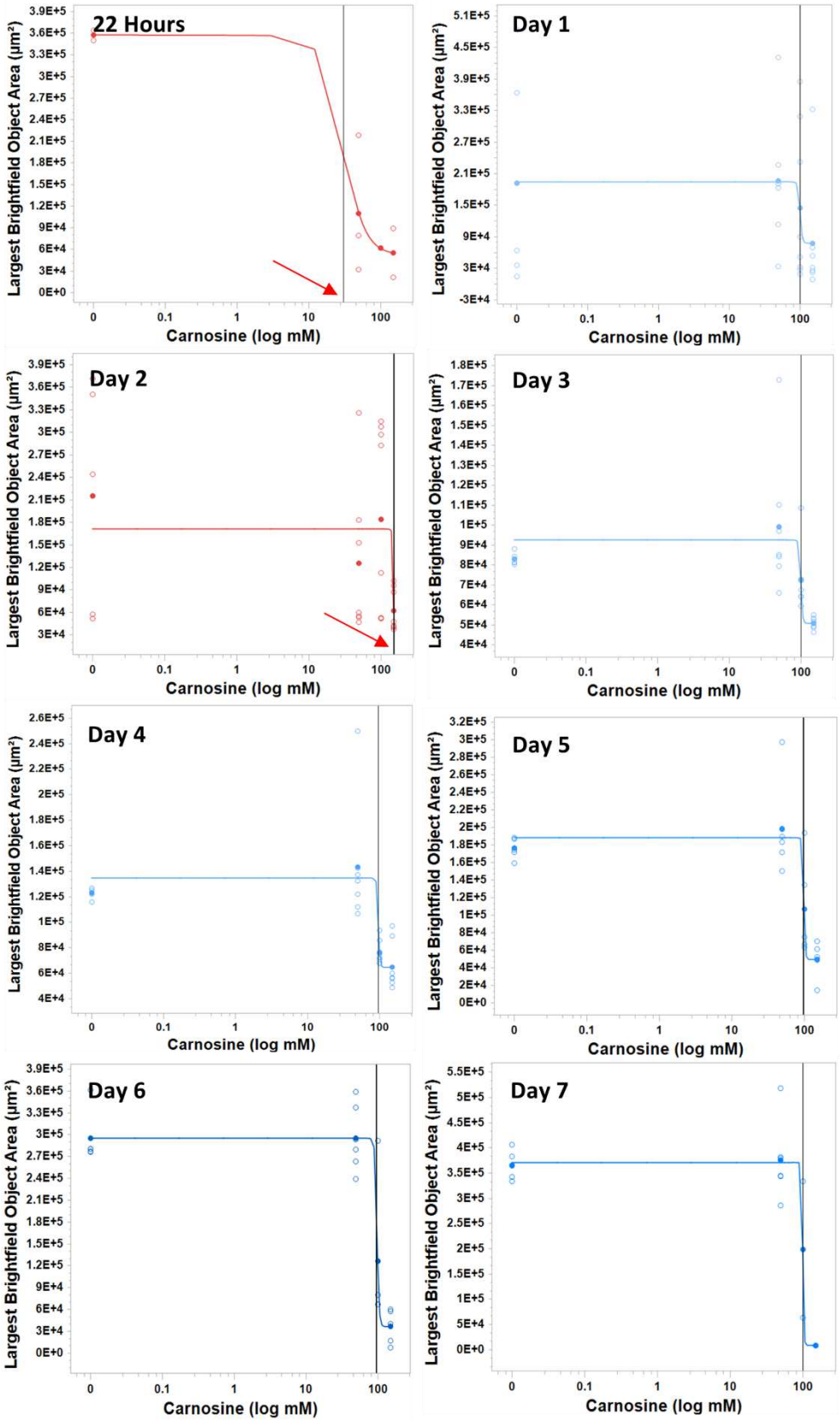

298

299 **Figure 8. IncuCyte S3 live-cell system (4×)** live spheroids images show the potential of using the protocol to
300 obtain EC50 of carnosine on multiple points for drug delivery study and *in vitro* sustained release profile. The
301 EC50 of carnosine on monolayer cells was calculated before day 1 spheroid for 7 days.

302 **Discussion**

303 Historically theranostic anticancer compounds were most often applied to cells grown in
304 monolayer, over the past decade sophisticated systems such as 3D cultures have been
305 developed to improve the prediction of clinical efficacy of compounds[23]. For example, Nunes
306 et. al 2019, formed 3D models of Glioblastoma Multiforme (GBM) tumor with tumor-
307 associated astrocytes microglia, endothelial cells, and immune cells. 3D models reproduce
308 cell-cell interactions, simulating the tumor microenvironment, these complex cell-cell
309 interactions are not present in 2D monolayer cell cultures, and this influences drug response[24].
310 Many advantages and disadvantages of tumor spheroid formation have been addressed from
311 popular methods[6,25]. Using ultra-low attachment well plates showed a strong similar intensity
312 to our method, which has been used to form several types of human and murine tumor
313 spheroids of various cell lines[6,7,26]. 3D tumor spheroids application included U87 MG, SEBTA-
314 027, SF188, DU-145, TRAMP-C1, BT-549, and Py230 cell lines. We found that it was essential
315 to use hydrophobic (non-wettable) polymer 96 well plates, as these plates make it difficult
316 for cells to attach to the bottom of the well. The red coded plates are modified so that they
317 have a hydrophilic surface which allows cells in serum-containing culture medium to adhere
318 and spread on the bottom of the well. However, the green coded plates with unmodified
319 polystyrene minimize the surface attachment effect and cell adherence[27,28]. Furthermore,
320 coating the surface of the wells with a film of zwitterionic material is an effective way to
321 reduce or eliminate nonspecific adsorption of the cells to the solid interface[19]. Cells were
322 allowed to assume a much rounder cylindrical morphology during the centrifuging process
323 when compared to the flatter morphology typically observed in the vessels (Fig 1 & 2).
324 Seeding at a density of 400 cells per well using 100 µl full media was optimized to obtain a
325 spheroid size of around 200 nm. Spheroids with a large average diameter > 200 µm are
326 exposed to large shear force, and as a result, it is impossible to form stable spheroid-spheroid
327 connections[6]. Moreover, we found that the speed of centrifugation played an important part
328 in forming tight spheroids as too low centrifugation speed led to the formation of
329 aggregates[9,30]. This allowed the cell-cell connection to be retained while inhibiting the cell-
330 well connection by the zwitterionic liquid wash. Since the plates were under orbital rotating,
331 cell collection was induced in the center of each well with even distribution by the centrifugal
332 forces[31]. Cell maturation was monitored using the IncuCyte live imaging system which allowed

333 viewing of the regular changes in each well. To image large single spheroids and avoid false-
334 negative data, IncuCyte spheroid software or z-stacks can be used[32]. In a previous report, the
335 liquid overlay method was performed on a 96-well plate and the equivalent diameter (range,
336 mean ± SD, CV%, n) of the obtained spheroids on day 7 was found to be within the range of
337 275 to 350 µm (mean 312 ± 23 µm, CV of 7.37%, n = 32)[26]. These results were close to those
338 obtained with the shaking separated cell sheets method within dispase-doped media after 9
339 to 12 days, seeding 800 cells/ petri dish at the start of the experiment. Indeed, the spheroids
340 were found to have a size ranging from 172 to 241 µm, (mean 201 ± 13 µm, CV of 6.35%, n =
341 460)[6]. Despite the high number of harvested spheroids from other methods, the protocol
342 detailed herein is better regarding the amount, uniformity, lowest deviation, and the fastest
343 preparation. Here, within 2 days and starting with 400 cells/ 100 µl per well using a 96 well
344 plate, the diameter of the harvested spheroids had a size range of 155 to 259 µm (mean 216
345 ± 9 µm, CV of 4.16%, n = 63) (Fig 2).

346 An easy method for mass production of homogeneous and uniform 3D cultures would lead to
347 a highly efficient sorting process that minimizes both setup time and wasted 3D cultures[33].
348 Utilizing the IncuCyte system and confocal imaging for 3D image analysis enabled the
349 characterization of the 3D cellular matrix of different spheroid phenotypes. The spheroids
350 were characterized by studying the 3D structures, cell viability, and necrosis. The presence of
351 dead cells in the spheroid center was due to hypoxia (Fig 2 & 3)[34]. Tumor hypoxia has been
352 attributed to tumorigenesis and therapeutic resistance by maintaining the undifferentiated
353 state of tumor stem cells. Thereby, therapeutic strategies should take oxygen tension into
354 account[34]. The loss of green CFSE fluorescent signal throughout the z depth of spheroids
355 exhibited a reproducible exponential decay function (Fig 3)[35]. Monitoring the changes in the
356 content of live, dead, and apoptotic cells enables observation of the consequences of
357 compound exposure on the spheroid[36]. Figure 4 displays the tightness of the generated
358 spheroids. The H&E staining of the middle cross-section of the spheroid encompassed the
359 complete tight structures from core to rim. The rim of the spheroid consisted of even layers
360 of packed cells toward the center despite the death of the cells which formed a necrotic core
361 region[37]. During spheroid formation, a small proportion of cells did not integrate into the
362 sphere and lost cell-cell adhesion properties. The reason for this separation is gravity-
363 sedimentation[38]. Western blotting revealed that spheroids generated after 10 days of culture

364 downregulated their expression of vimentin, albeit not significant when compared to cells
365 grown in monolayer. The downregulation of vimentin further indicates that cells within these
366 spheroids appear to adopt a stem cell phenotype. The previous process of validation
367 confirmed that the employed procedure is suitable for its intended use. The reported results
368 addressed the quality, reliability, and consistency of optimal *in vitro* 3D-model generation
369 relying on a robust and cost-effective protocol.

370 The penetration and binding of compounds into spheroids have been shown to be a promising
371 predictor of compound uptake in thick tissues[39]. The formed tumor spheroids of U87 MG
372 reflected the effect concentration EC50 by using carnosine as a treatment[40]. By utilizing
373 different concentrations (0, 50, 100, 150 mM) of carnosine in a sustained release designed
374 experiment, the inhibition of the single spheroids' growth was significant compared to
375 untreated spheroids[15]. Generating single spheroids from seven different murine and human
376 tumor cell lines showed the potential of this method for generating spheroids from various
377 cancer types (brain, prostate, and breast) starting with the same cell density per well (Fig 6).
378 The size of the spheroids can be adjusted by seeding different cell numbers and manipulating
379 the time of incubation according to the personalized experiment design. One should however
380 keep in mind that the core region consisting of a necrotic area will also increase with the
381 spheroid size and therefore experiments aiming to assess treatment efficacy will have to be
382 carefully planned[41]. After the optimization towards mimicking various stages of avascular
383 tumor regions, the resulting single spheroids can easily be transferred to any plate or cell
384 culture vessel due to the ease of mechanical access for further investigation or analysis. Cell
385 viability assays such as the MTT, trypan blue exclusion, and LDH release assays can be used
386 for *in vitro* therapeutic screening in spheroids[23]. Consistent culture conditions need to be kept
387 during the spheroid growth as this otherwise might affect proliferation significantly by
388 altering the expression of tight junction molecules, which establish a delay in the initial
389 shrinking of the spheroid size[7] . On average the spheroids reach a stable symmetrical size after
390 24 to 48 hours post-seeding. However, some cell lines require a longer time such as the DU145
391 cells which needed around 5 days to produce firm spheroids. The observed diameter was *ca.*
392 200 nm at which the spheroids started to show a necrotic core and a proliferative outer layer.
393 In the future, adding cells of the tumor microenvironment to develop multicellular 3D cultures

394 will make the models more representative of the *in vivo* tumor situation[42] . This protocol could
395 also be tested on essential tumor stem cells such as SJ-1.[34]

396 **Conclusion**

397 Monolayer cultured tumor cells exhibit less resistance to therapeutic interventions than *in*
398 *vivo* cells. Developing a 3D model that more resembles solid tumors is important, especially
399 when trying to bridge the gap between *in vitro* and *in vivo* tumor models. The use of 3D
400 models is nowadays largely diffused, and the commonly used protocols were followed by
401 significant updates. The protocol described here demonstrated reproducible findings in
402 generating robust single spheroids using a simple cost-effective method that other
403 researchers and different laboratories can benefit from. Indeed, uniform single spheroids
404 without any additives were consistently obtained. The spheroids exhibited the typical
405 characteristic morphology consisting of a proliferating rim and a necrotic core. These can then
406 be used to assess drugs EC50 as was highlighted using carnosine treatment. Preliminary
407 optimization for different cell lines of single spheroids is proposed to provide the research
408 workers with an easily accessible and average 20-fold cheaper method than the ultra-low
409 adherent plates for *in vitro* investigating. In the future, the reported data needs to be further
410 studied to find the validity of patient-derived tumor cells.

411 **Author Contributions:** K.H. contributed to experimental design, performed the experiments,
412 and wrote the first draft, J.R.D.P. performed the Western blot experiment and contributed to
413 the final manuscript, and S.E.B.M. contributed to the final manuscript. All authors have read
414 and agreed to the published version of the manuscript.

415 **Funding:** This work was supported by Nottingham Trent University and CARA (Council for At-
416 Risk Academics) fellowship program.

417 **Data Availability Statement:** The data presented in this study are available on request from
418 the corresponding author.

419 **Acknowledgments:** The authors would like to acknowledge Dr. Graham Hickman for his
420 technical support with the electron microscopy studies. Also, the authors appreciate the
421 efforts of Gareth Williams in the guidance of histology work. K.H. would like to thank the
422 Nottingham Trent University & CARA fellowship program for the generous award and support.

423 **Conflicts of Interest:** The authors declare no conflict of interest.

424 **References**

425 1. Ravi, M., Paramesh, V., Kaviya, S. R., Anuradha, E. & Paul Solomon, F. D. 3D Cell
426 Culture Systems: Advantages and Applications. *J Cell. Physiol*. **230**, 16–26 (2015).
427 2. Kunz-Schughart, L. A. Multicellular tumor spheroids: intermediates between
428 monolayer culture and in vivo tumor. *Cell Biol. Int*. **23**, 157–161 (1999).
429 3. LaBarbera, D. v., Reid, B. G. & Yoo, B. H. The multicellular tumor spheroid model
430 for high-throughput cancer drug discovery. *Expert Opin. Drug Discovery.* **7**, 819–
431 830 (2012).
432 4. Carlsson, J. & Yuhas, J. M. Liquid-Overlay Culture of Cellular Spheroids. Recent
433 results in cancer research. *Recent Results Cancer Res.* **95**, 1–23 (1984).
434 5. Timmins, N., Dietmair, S. & Nielsen, L. Hanging-drop multicellular spheroids as a
435 model of tumour angiogenesis. *Angiogenesis*. **7**, 97–103 (2004).
436 6. Shi, W. et al. Facile Tumor Spheroids Formation in Large Quantity with Controllable
437 Size and High Uniformity. *Sci. Rep*. **8**, 1–9 (2018).
438 7. Ivascu, A. & Kubbies, M. Rapid Generation of Single-Tumor Spheroids for High-
439 Throughput Cell Function and Toxicity Analysis. *SLAS Discovery.* **8**, 922–932 (2006).
440 8. Haisler, W. L. et al. Three-dimensional cell culturing by magnetic levitation. *Nat.*
441 *Protoc*. **8**, 1940–1949 (2013).
442 9. Hammond, T. G. & Hammond, J. M. Optimized suspension culture: The rotating-
443 wall vessel. *Am. J. Physiol*. **281**, (2001).
444 10. He, Y. et al. Fabrication of micro-cages and caged tumor spheroids for microfluidic
445 chip-based assays. *Microelectron. Eng*. **225**, 111256 (2020).
446 11. Winter, G., Griffiths, A. D., Hawkins, R. E. & Hoogenboom, H. R. Making Antibodies
447 by Phage Display Technology.
448 http://dx.doi.org/10.1146/annurev.iy.12.040194.002245 12, 433–455 (2003).
449 12. Qiang, L. et al. Isolation and characterization of cancer stem like cells in human
450 glioblastoma cell lines. *Cancer Lett*. **279**, 13–21 (2009).
451 13. Allen, M., Bjerke, M., Edlund, H., Nelander, S. & Westermark, B. Origin of the
452 U87MG glioma cell line: Good news and bad news. *Sci. Transl. Med*. **8**, (2016).

453 14. Pontén, J. & Macintyre, E. H. Long term culture of normal and neoplastic human
454 glia. *Acta Pathol. Microbiol. Scand*. **74**, 465–486 (1968).
455 15. Habra, K., McArdle, S. E. B., Morris, R. H. & Cave, G. W. V. Synthesis and
456 Functionalisation of Superparamagnetic Nano-Rods towards the Treatment of
457 Glioblastoma Brain Tumours. *Nanomaterials*. **11**, 2157 (2021).
458 16. Trédan, O., Galmarini, C. M., Patel, K. & Tannock, I. F. Drug Resistance and the Solid
459 Tumor Microenvironment. *JNCI, J. Natl. Cancer Inst*. **99**, 1441–1454 (2007).
460 17. Overview of old/new article numbers of Sarstedt TC flasks, plates, and dishes.
461 https://www.sarstedt.com/fileadmin/user_upload/99_Broschueren/Englisch_US
462 _Code/667_tc_produkte_alt_neu_USA_1014.pdf (2022).
463 18. Spheroid | Sartorius. https://www.sartorius.com/en/applications/life-science-
464 research/cell-analysis/live-cell-assays/assays-for-3d-models/spheroid-
465 growth/spheroid (2022).
466 19. Schlenoff, J. B. Zwitteration: Coating surfaces with zwitterionic functionality to
467 reduce nonspecific adsorption. *Langmuir.* **30**, 9625–9636 (2014).
468 20. Iwadate, Y. Epithelial-mesenchymal transition in glioblastoma progression. *Oncol.*
469 *Lett.* **11**, 1615–1620 (2016).
470 21. Essid, N., Chambard, J. C. & Elgaaïed, A. B. Induction of epithelial-mesenchymal
471 transition (EMT) and Gli1 expression in head and neck squamous cell carcinoma
472 (HNSCC) spheroid cultures. *Bosnian J. Basic Med. Sci.* **18**, 336 (2018).
473 22. Lathia, J. D., Mack, S. C., Mulkearns-Hubert, E. E., Valentim, C. L. L. & Rich, J. N.
474 Cancer stem cells in glioblastoma. Genes Dev. **29**, 1203–1217 (2015).
475 23. Daunys, S., Janonienė, A., Januškevičienė, I., Paškevičiūtė, M. & Petrikaitė, V. 3D
476 Tumor Spheroid Models for In Vitro Therapeutic Screening of Nanoparticles. *Adv.*
477 *Exp. Med. Biol*. **1295**, 243–270 (2021).
478 24. Nunes, A. S., Barros, A. S., Costa, E. C., Moreira, A. F. & Correia, I. J. 3D tumor
479 spheroids as in vitro models to mimic in vivo human solid tumors resistance to
480 therapeutic drugs. *Biotechnol. Bioeng.* **116**, 206–226 (2019).
481 25. Kim, S. J., Kim, E. M., Yamamoto, M., Park, H. & Shin, H. Engineering Multi-Cellular
482 Spheroids for Tissue Engineering and Regenerative Medicine. *Adv. Healthcare*
483 *Mater*. **9**, 2000608 (2020).

484 26. Zanoni, M. et al. 3D tumor spheroid models for in vitro therapeutic screening: a
485 systematic approach to enhance the biological relevance of data obtained. *Sci. Rep*.
486 **6**, 1–11 (2016).
487 27. Raey, W. S., Hertl, W., Nowlan, E. D. & Binkowski, N. J. Surface treatments and cell
488 attachment. *In Vitro***. 20**, 802–808 (1984).
489 28. Curtis, A. S. G., Forrester, J. v., McInnes, C. & Lawrie, F. Adhesion of cells to
490 polystyrene surfaces. *J. Cell Biol*. **97**, 1500–1506 (1983).
491 29. Efremov, Y. M. et al. Mechanical properties of cell sheets and spheroids: the link
492 between single cells and complex tissues. *Biophys. Rev*. **13**, 541–561 (2021).
493 30. Kalantarian, A. et al. Axisymmetric Drop Shape Analysis for Estimating the Surface
494 Tension of Cell Aggregates by Centrifugation. *Biophys. J.* **96**, 1606–1616 (2009).
495 31. Park, J., Lee, G. H., Yull Park, J., Lee, J. C. & Kim, H. C. Hypergravity-induced
496 multicellular spheroid generation with different morphological patterns precisely
497 controlled on a centrifugal microfluidic platform. *Biofabrication.* **9**, 045006 (2017).
498 32. Lugagne, J. B. et al. Identification of individual cells from z-stacks of bright-field
499 microscopy images. *Sci. Rep*. **8**, 1–5 (2018).
500 33. Leu, M. P., Calatayud, N., Smet, F., Comas, A. & Thomsen, A. Easy mass production
501 of homogenous and uniform 3D spheroids for high-throughput screening
502 applications. https://www.chayon.co.kr/wp-content/uploads/2021/02/MPLeu-
503 et-al-V17-20200703.pdf (2020).
504 34. Kolenda, J. et al. Effects of hypoxia on expression of a panel of stem cell and
505 chemoresistance markers in glioblastoma-derived spheroids. *J. Neuro-Oncol*. **103**,
506 43–58 (2011).
507 35. Leary, E., Rhee, C., Wilks, B. T. & Morgan, J. R. Quantitative Live-Cell Confocal
508 Imaging of 3D Spheroids in a High-Throughput Format. *SLAS Technol.* **23**, 231–242
509 (2018).
510 36. Sirenko, O. et al. Phenotypic characterization of toxic compound effects on liver
511 spheroids derived from ipsc using confocal imaging and three-dimensional image
512 analysis. *Assay Drug Dev. Technol*. **14**, 381–394 (2016).
513 37. Bull, J. A., Mech, F., Quaiser, T., Waters, S. L. & Byrne, H. M. Mathematical
514 modelling reveals cellular dynamics within tumour spheroids. *PLoS Comput. Biol*.
515 **16**, e1007961 (2020).

516 38. Stadler, M. et al. Exclusion from spheroid formation identifies loss of essential cell-
517 cell adhesion molecules in colon cancer cells. *Sci. Rep*. **8**, 1–16 (2018).
518 39. Hjelstuen, M. H., Rasch-Halvorsen, K., Brekken, C., Bruland, Ø. & Davies, C. D. L.
519 Penetration and Binding of Monoclonal Antibody in Human Osteosarcoma
520 Multicell Spheroids: Comparison of confocal laser scanning microscopy and
521 autoradiography. *Acta Oncol*. **35**, 273–279 (2009).
522 40. Habra, K., Morris, R. H., St´, S., Mcardle, S. E. B. & Cave, G. W. v. Controlled release
523 of carnosine from poly(lactic- co -glycolic acid) beads using nanomechanical
524 magnetic trigger towards the treatment of glioblastoma. *Nanoscale Adv.* **4**, 2242-
525 2249 (2022).
526 41. Carlsson, J. et al. Formation and growth of multicellular spheroids of human origin.
527 *Int. J. Cancer*. **31**, 523–533 (1983).
528 42. Zraikat, M. & Alshelleh, T. Comparison Between Different 3D Spheroid Tumor
529 Invasion Models. *Assay Drug Dev. Technol.* **18**, 239–242 (2020).

Supplementary Files

This is a list of supplementary files associated with this preprint. Click to download.

- supplimentaryInfo.pdf